

Anfinsen Goes Neural: a Graphical Model for Conditional Antibody Design

Nayoung Kim¹ Minsu Kim¹ Jinkyoo Park¹

Abstract

Antibody design plays a pivotal role in advancing therapeutics. Although deep learning has made rapid progress in this field, existing methods make limited use of general protein knowledge and assume a graphical model (GM) that violates empirical findings on proteins. To address these limitations, we present Anfinsen Goes Neural (AGN), a graphical model that uses a pre-trained protein language model (pLM) and encodes a seminal finding on proteins called Anfinsen’s dogma. Our framework follows a two-step process of sequence generation with pLM and structure prediction with graph neural network (GNN). Experiments show that our approach outperforms state-of-the-art results on benchmark experiments. We also address a critical limitation of non-autoregressive models – namely, that they tend to generate unrealistic sequences with overly repeating tokens. To resolve this, we introduce a composition-based regularization term to the cross-entropy objective that allows an efficient trade-off between high performance and low token repetition. We demonstrate that our approach establishes a Pareto frontier over the current state-of-the-art. Our code is available at <https://github.com/lkny123/AGN>.

1. Introduction

Monoclonal antibodies are one of the most promising drug modalities (Jin et al., 2022a) that treat diseases by binding specifically to the disease-causing agent with complementarity-determining regions (CDRs). This implies that the ability to design CDRs with desired properties can unleash the potential to treat many diseases.

Recently, the deep learning community has devoted much attention to antibody design. Early models focused solely on designing the CDR *sequences* (Liu et al., 2020; Saka et al., 2021; Akbar et al., 2022), which obscured how the

structure of antibodies made them functional (Martinkus et al., 2023). As an alternative, Jin et al. (2021) proposed the *sequence-structure co-design* task, where the goal is to generate both the CDR sequence and the corresponding CDR structure. Many works made notable progress on this task, including Jin et al. (2021), Jin et al. (2022b), Kong et al. (2022), and Verma et al. (2023).

Despite this progress, we claim that previous approaches to sequence-structure co-design are suboptimal due to three major limitations:

- (1) **Limited use of general protein knowledge.** Previous models are trained on the SAbDab dataset ($\sim 8 \times 10^3$) (Dunbar et al., 2014), which is much smaller than the general protein dataset such as UniRef-50 ($\sim 6 \times 10^7$) (Suzek et al., 2015). This inevitably leads to overfitting and poor generalization, and thus a low-quality design for unseen antibodies. We emphasize that antibodies are still subsets of proteins, so utilizing general protein knowledge as a prior may improve design quality.
- (2) **Violation of Anfinsen’s dogma.** A model should be constructed in a way that coincides with empirical findings. One of the seminal findings on proteins is Anfinsen’s dogma (Anfinsen, 1973), a noble-Prize-winning postulate in molecular biology:

The native conformation [of a protein] is determined ... by the amino acid sequence, in a given environment.

Anfinsen’s dogma guides us to model the data-generating process as (sequence \mathbf{s}) \rightarrow (structure \mathbf{x}), where we first design the sequence \mathbf{s} then use the sequence to predict the structure \mathbf{x} .

However, previous graph neural network (GNN)-based models (Jin et al., 2021; 2022b; Kong et al., 2022) (Figure 1A) ignore this causal view by (1) assuming a common latent factor $\mathbf{h}_{\mathbf{s}, \mathbf{x}}$ that *jointly* generates both sequence and structure and (2) allowing the sequence to depend on initialized structure \mathbf{x}_0 . In this paper, we demonstrate that such violations of Anfinsen’s dogma lead to sub-optimal task performance.

- (3) **Token repetition of non-autoregressive models.**

Recent works show that non-autoregressive decomposition of sequences not only exhibits faster inference

¹Korea Advanced Institute of Science and Technology. Correspondence to: Nayoung Kim <lkny123@kaist.ac.kr>.

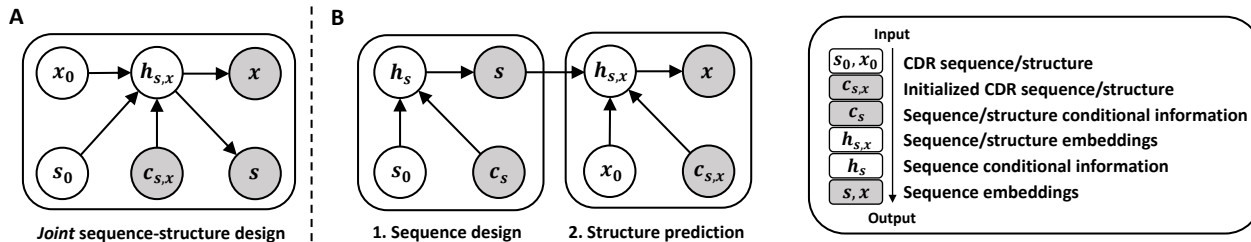


Figure 1. Graphical models (GMs) for sequence-structure co-design. Shaded nodes represent the data. (A) GM of previous GNN-based methods tackling sequence-structure co-design. The underlying assumption violates Anfinsen’s dogma by assuming a common latent factor $h_{s,x}$ and allowing the flow $x_0 \rightarrow s$. (B) Our GM adopts the causal view $s \rightarrow x$ following Anfinsen’s dogma.

speed but also achieves state-of-the-art performance on many protein design tasks (Gao et al., 2022; Zheng et al., 2023; Kong et al., 2022). Nevertheless, the complete conditional independence assumption promotes non-autoregressive models to produce repeated tokens (Gu et al., 2017; Ghazvininejad et al., 2019). This results in a non-realistic antibody sequence (Jin et al., 2021), a problem that must be addressed for a real-world application of antibody design models.

We propose Anfinsen Goes Neural (AGN), a two-step graphical model that first generates CDR sequence s with a fine-tuned protein language model (pLM) and predicts the corresponding structure x with a GNN-based model (Figure 1B). AGN overcomes problem (1) by leveraging pre-trained pLM, whose sequential evolutionary knowledge can kickstart the learning process for antibody sequence design, and resolves problem (2) by adopting the causal view $s \rightarrow x$ of Anfinsen’s dogma.

To resolve problem (3), we propose a composition-based regularization term to the conventional cross-entropy sequence loss. The proposed term forces the predicted sequences to be compositionally similar to natural protein sequences, effectively reducing token repetition.

We highlight our main contributions as follows:

- We introduce AGN, a framework that leverages general protein knowledge of pLM and satisfies Anfinsen’s dogma (Section 4, Section 5) for optimal performance.
- We propose a composition-based regularization term that prevents non-autoregressive models from generating overly repetitive tokens (Section 5) and demonstrate the effectiveness of this approach experimentally (Section 7).
- We demonstrate that AGN outperforms state-of-the-art models on all benchmark experiments (Section 6). Specifically, we improve amino acid recovery (AAR) and root mean squared deviation (RMSD) by 8.38 – 27.12% and 1.12 – 12.60% on Sequence and Structure Modeling (Section 6.1); 8.88% and 1.59% on Antigen-binding CDR-H3 Design (Section 6.2).

2. Related Work

Physics-based methods are the earliest approach to antibody design (Pantazes & Maranas, 2010; Li et al., 2014; Lapidot et al., 2015; Adolf-Bryfogle et al., 2018). These methods require iterative Monte Carlo simulations to find sequences and structures with minimum binding energy, which makes them computationally expensive.

Deep learning-based methods offer a strong alternative with both faster computation and greater modeling flexibility. Many pioneering works (Liu et al., 2020; Saka et al., 2021; Akbar et al., 2022) design only 1D sequences using CNN and LSTM. Recently, Melnyk et al. (2022) showed improved 1D sequence modeling performance by repurposing a pre-trained Transformer-based English language model for sequence infilling. Similar to our work, they also fine-tune protein language models for antibody sequence design; however, our work differs in that we provide a framework for modeling both 1D sequence and 3D structure and address the token repetition problem of non-autoregressive models.

Instead of designing only 1D sequences, Jin et al. (2021) proposes sequence-structure co-design, which involves both 1D sequence and 3D structure infilling of CDRs. Specifically, Jin et al. (2021) represents the antibody-antigen complex with an E(3)-invariant graph and predicts the sequence in an autoregressive fashion. On the contrary, Kong et al. (2022) constructs an E(3)-equivariant graph to fully capture the 3D geometry and predicts sequence by a full-shot decoding scheme to speed up inference. Verma et al. (2023) formulates a coupled neural ODE system over the antibody nodes and further increases inference speed with a single round of full-shot decoding. Unlike deterministic GNN-based methods, Luo et al. (2022) and Martinkus et al. (2023) adopt diffusion probabilistic models to generate structures stochastically. Notably, Martinkus et al. (2023) supports their approach with laboratory experiments.

Please refer to Appendix A for related work on protein design and protein language models.

3. Preliminaries, Notations, and Task Formulation

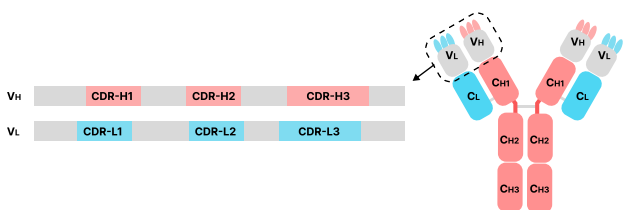


Figure 2. Schematic structure of an antibody. Our goal is to design heavy chain CDRs, regions that contribute the most to antibody-antigen interaction.

Preliminaries. An antibody consists of a pair of light chains and heavy chains (Figure 2). Both the light chain and heavy chain are composed of a variable region (V_L ; V_H) and constant region(s) (C_L ; C_{H1} , C_{H2} , C_{H3}). Each variable region could be further decomposed into three complementarity-determining regions (CDR-L1, CDR-L2, CDR-L3; CDR-H1, CDR-H2, CDR-H3) and a framework region, which is the complement of CDRs. Following Jin et al. (2021), we narrow the scope of our task to sequence-structure co-design of heavy chain CDRs as they contribute the most to antibody-antigen interaction.

Notations. Let L be the number of residues in CDR. We denote the *ground-truth* sequence and structure of a heavy chain CDR as $\mathbf{s} = (s_1, \dots, s_L)$ and $\mathbf{x} = (x_1, \dots, x_L)$ and the *predicted* sequence and structure as $\hat{\mathbf{s}} = (\hat{s}_1, \dots, \hat{s}_L)$ and $\hat{\mathbf{x}} = (\hat{x}_1, \dots, \hat{x}_L)$. We also denote the conditional information (e.g., framework region and/or antigen) as $\mathbf{c}_{\mathbf{s}, \mathbf{x}}$ if it contains both sequential and structural information and $\mathbf{c}_{\mathbf{s}}$ if it contains only sequential information. Throughout the text, we use the terms context and conditional information interchangeably.

Task formulation. Given the context $\mathbf{c}_{\mathbf{s}, \mathbf{x}}$, our goal is to train $p_{\theta}(\mathbf{s}, \mathbf{x} | \mathbf{c}_{\mathbf{s}, \mathbf{x}})$ that generates a suitable CDR sequence \mathbf{s} and the corresponding structure \mathbf{x} . Most antibody design models additionally use initialized sequence \mathbf{s}_0 and structure \mathbf{x}_0 as inputs, in which case the goal is to train $p_{\theta}(\mathbf{s}, \mathbf{x} | \mathbf{s}_0, \mathbf{x}_0, \mathbf{c}_{\mathbf{s}, \mathbf{x}})$. We adhere to the latter formulation throughout the paper.

4. Overall Pipeline of AGN

During the forward pass, AGN generates a CDR sequence \mathbf{s} and structure \mathbf{x} , given the context $\mathbf{c}_{\mathbf{s}, \mathbf{x}}$ and initializations \mathbf{s}_0 and \mathbf{x}_0 . As a result of graph surgery in Appendix B, the AGN pipeline (Figure 1B) consists of two steps: (1) **sequence design** and (2) **structure prediction**. Each step is composed of two simple sub-steps: (A) *initialize* and (B) *sample*. The overview of our model is shown in Figure 3.

4.1. Step 1: Sequence Design

In **Step 1**, we use a fine-tuned ESM2 (Lin et al., 2023) – the state-of-the-art pLM – to design CDR sequence \mathbf{s} from the initialized sequence \mathbf{s}_0 (orange in Figure 3) and context sequence $\mathbf{c}_{\mathbf{s}}$ (white in Figure 3).

- Initialize* the CDR sequence \mathbf{s} to \mathbf{s}_0 by replacing all the tokens with mask token ($\langle MASK \rangle$), which serves as a placeholder for token positions that need to be predicted.
- Sample* the CDR sequence $\hat{\mathbf{s}} = (\hat{s}_1, \dots, \hat{s}_L)$ from a fine-tuned protein language model $p_{\theta}(\mathbf{s} | \mathbf{s}_0, \mathbf{c}_{\mathbf{s}})$. Following the original implementation of ESM2 (Lin et al., 2023), we assume conditional independence between the tokens – i.e., $p_{\theta}(\mathbf{s} | \mathbf{s}_0, \mathbf{c}_{\mathbf{s}}) = \prod_{i=1}^L p_{\theta}(s_i | \mathbf{s}_0, \mathbf{c}_{\mathbf{s}})$.

4.2. Step 2: Structure Prediction

In **Step 2**, we adopt MEAN (Kong et al., 2022) as our structure prediction model to predict the CDR structure \mathbf{x} from sampled sequence $\hat{\mathbf{s}}$, initialized structure \mathbf{x}_0 , and context $\mathbf{c}_{\mathbf{s}, \mathbf{x}}$. By using the sampled sequence $\hat{\mathbf{s}}$ to generate $\hat{\mathbf{x}}$, we effectively exploit the causal relationship $\mathbf{s} \rightarrow \mathbf{x}$ derived from Anfinsen’s dogma.

- Initialize* the graph $\mathcal{G}(\hat{\mathbf{s}}, \mathbf{x}_0, \mathbf{c}_{\mathbf{s}, \mathbf{x}})$ from predicted CDR sequence $\hat{\mathbf{s}}$, initialized CDR coordinates \mathbf{x}_0 , and conditional information $\mathbf{c}_{\mathbf{s}, \mathbf{x}}$. Each node corresponds to a residue and is assigned with an amino acid embedding and coordinates of backbone atoms N, C_{α}, C, O . For node v_i in the CDR region, we assign the embeddings of \hat{s}_i and the initialized backbone coordinates $\hat{x}_{0,i}$ sampled from nearby residues. We also construct two types of edges – \mathcal{E}_{in} and \mathcal{E}_{out} . Specifically, \mathcal{E}_{in} is a set of internal edges between the residues within the same polypeptide chain and a distance cutoff of c_1 . On the other hand, \mathcal{E}_{out} is a set of external edges between residues in different chains and within a distance cutoff of $c_2 > c_1$. For more details about graph construction, we refer the readers to Kong et al. (2022).
- Sample* the corresponding CDR structure from MEAN as $\hat{\mathbf{x}} \sim p_{\phi}(\hat{\mathbf{x}}, \mathbf{x} | \mathcal{G}(\hat{\mathbf{s}}, \mathbf{x}_0, \mathbf{c}_{\mathbf{s}, \mathbf{x}}))$. Unlike the original implementation, we here feed MEAN with generated sequence $\hat{\mathbf{s}}$ instead of the initialized sequence \mathbf{s}_0 and use only the structure output \mathbf{x} while discarding the sequence output.

5. Training AGN

Our goal is find Θ^* that maximizes the log-likelihood objective:

$$\Theta^* = \arg \max \mathbb{E}_{(\mathbf{x}, \mathbf{s}, \mathbf{c}_{\mathbf{s}, \mathbf{x}}) \sim p_{\mathcal{D}}} [\log p_{\Theta}(\mathbf{s}, \mathbf{x} | \mathbf{s}_0, \mathbf{x}_0, \mathbf{c}_{\mathbf{s}, \mathbf{x}})] \quad (1)$$

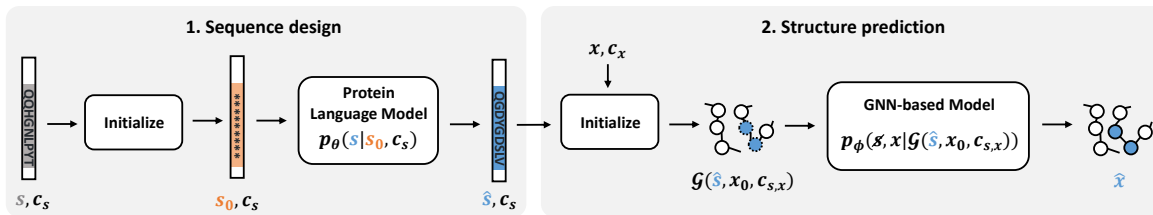


Figure 3. Overview of AGN pipeline. During the forward pass, AGN generates CDR sequence and structure \hat{s}, \hat{x} from initializations s_0, x_0 and context $c_{s,x}$. The forward pass consists of two steps: (1) sequence design and (2) structure prediction. Each step can be decomposed into two sub-steps: (A) initializing sequence/structure and (B) sampling sequence/structure, respectively.

where p_D is the data distribution. Based on the GM in Figure 1B, $\log p_\Theta(\mathbf{s}, \mathbf{x}|s_0, \mathbf{x}_0, \mathbf{c}_{s,x})$ factorizes into two terms:

$$\begin{aligned} \log p_\Theta(\mathbf{s}, \mathbf{x}|s_0, \mathbf{x}_0, \mathbf{c}_{s,x}) \\ = \underbrace{\log p_\theta(\mathbf{s}|s_0, \mathbf{c}_s)}_{(1) \text{ Seq. Obj.}} + \underbrace{\log p_\phi(\mathbf{x}|\mathbf{s}, \mathbf{x}_0, \mathbf{c}_{s,x})}_{(2) \text{ Struct. Obj.}} \end{aligned} \quad (2)$$

Following this factorization, we first derive the fine-tuning objective for pre-trained pLM in Section 5.1, followed by the objective for GNN-based structure prediction model in Section 5.2.

5.1. Training Sequence Design Model

To train a sequence design model, we (1) *pre-train* a general protein language model (pLM) on the UniRef-50D dataset and (2) *fine-tune* it on the SAbDab dataset. With this approach, we can utilize the sequential evolutionary knowledge of pre-trained pLMs to kickstart the learning process for antibody sequence design, preventing overfitting on a relatively small antibody dataset.

Pre-training objective. A common pre-training objective for pLMs is the masked language modeling (MLM) objective (Devlin et al., 2018; Rives et al., 2019). Let \mathbf{s} temporarily denote a general protein sequence (not CDR sequence) and $p_D(\mathbf{s})$ denote the empirical data distribution of UniRef-50D. The MLM objective is given by:

$$\mathcal{L}_{\text{MLM}}(\theta) = \mathbb{E}_{\mathbf{s} \sim p_D(\mathbf{s})} \sum_{i \in M} -\log p_\theta(s_i | \mathbf{s}_{\setminus M}) \quad (3)$$

where $M \subset \{1, \dots, L\}$ is the set of indices selected for corruption. Specifically, M refers to 15% of randomly selected tokens that are either (1) replaced with $\langle \text{MASK} \rangle$ with 80% probability, (2) randomly altered with 10% probability, or (3) left intact with 10% probability. For more details, we refer the readers to Rives et al. (2019).

Fine-tuning objective. Here, we derive the exact form of the fine-tuning sequence objective $\log p_\theta(\mathbf{s}|s_0, \mathbf{c}_s)$. The non-autoregressive factorization of the sequence objective is: $\mathcal{L}(\theta) = -\log p_\theta(\mathbf{s}|s_0, \mathbf{c}_s) = -\sum_{i=1}^L \log p_\theta(s_i | s_0, \mathbf{c}_s)$. However, the complete conditional independence assumption between s_i allows the model to generate repetitive tokens (Gu et al., 2017; Ghazvininejad et al., 2019).

To reduce token repetition, we highlight the following observation: *if the tokens are highly repetitive (e.g., AR-GYYYYYYY), then the sequence will be compositionally different from the natural protein sequence.* Accordingly, we add a regularization term to the MLE objective:

$$\mathcal{L}(\theta) = -\sum_{i=1}^L \log p_\theta(s_i | s_0, \mathbf{c}_s) + \underbrace{\alpha \cdot \mathbb{E}_{\hat{\mathbf{s}}} [d(\mathbf{s}, \hat{\mathbf{s}})]}_{\text{Regularization}} \quad (4)$$

where $\hat{\mathbf{s}} \sim p_\theta(\mathbf{s}|s_0, \mathbf{c}_s)$ and $d(\mathbf{s}, \hat{\mathbf{s}})$ measures the cosine similarity between the composition vectors \mathbf{y}_s and $\mathbf{y}_{\hat{\mathbf{s}}}$ defined as $(\mathbf{y}_s)_j = \sum_{i=1}^L \mathbb{I}(s_i = \mathcal{A}_j), \forall j \in \{1, \dots, |\mathcal{A}|\}$ with \mathcal{A} denoting the set of residue types. Since this objective forces the model to design sequences compositionally similar to natural sequences, by the contrapositive of our observation statement, we can expect less repetitive sequences.

Implementation. We adopt ESM2-650M (Lin et al., 2023), the state-of-the-art protein language model, as the starting point of our sequence design model. Due to memory limitations, we fine-tune it with the low-rank adaptation technique (LoRA) (Hu et al., 2021) using rank 2 for weights W_q, W_k, W_v , and W_o in the multi-head attention module. We choose the heavy chain framework region as the context sequence c_s since including the antigen sequence did not improve the results (Appendix D). To implement the fine-tuning objective in Equation (4), we express the first term as the cross-entropy loss $\sum_{i=1}^L \ell_{\text{ce}}(s_i, \mathbf{p}_i)$, where \mathbf{p}_i is the language head output of ESM2. Specifically, given the ESM2 embeddings $\mathbf{h}_s = (\mathbf{h}_{s,1}, \dots, \mathbf{h}_{s,L})$ of CDR residues, the \mathbf{p}_i is parameterized as $\mathbf{p}_i = \text{Linear}(\text{LayerNorm}(\text{GELU}(\text{Linear}(\mathbf{h}_{s,i}))))$ (Ba et al., 2016; Hendrycks & Gimpel, 2016; Rives et al., 2021; Lin et al., 2023). The second term is implemented with the score function estimator (Fu et al., 2015); by using the log-derivative trick, the *gradient* of this term is given by $\mathbb{E}_{\hat{\mathbf{s}} \sim p_\theta(\mathbf{s}|s_0, \mathbf{c}_s)} [d(\mathbf{s}, \hat{\mathbf{s}}) \nabla_\theta \log p_\theta(\mathbf{s}|s_0, \mathbf{c}_s)]$. With single sample Monte Carlo approximation, the final training objective is:

$$\mathcal{L}(\theta) = \sum_{i=1}^L \ell_{\text{ce}}(s_i, \mathbf{p}_i) + \alpha \cdot d(\mathbf{s}, \hat{\mathbf{s}}) \log p_\theta(\mathbf{s}|s_0, \mathbf{c}_s) \quad (5)$$

Although this objective is written with respect to a single datapoint, in practice, we work in batches and use the batch

Table 1. AAR(\uparrow) and RMSD(\downarrow) on SABDab dataset for Sequence and Structure Modeling. AGN outperforms baselines on both metrics.

	CDR-H1		CDR-H2		CDR-H3	
	AAR (%)	RMSD	AAR (%)	RMSD	AAR (%)	RMSD
LSTM	39.47 \pm 2.11	-	30.41 \pm 2.47	-	15.82 \pm 1.63	-
AR-GNN	48.39 \pm 4.72	2.904 \pm 0.1651	38.03 \pm 2.81	2.295 \pm 0.1574	18.72 \pm 0.82	3.598 \pm 0.577
RefineGNN	42.03 \pm 2.88	0.8723 \pm 0.1013	32.05 \pm 2.23	0.7942 \pm 0.0645	24.44 \pm 1.94	2.243 \pm 0.139
MEAN	59.32 \pm 4.71	0.9108 \pm 0.0994	48.85 \pm 2.32	0.8756 \pm 0.0709	36.50 \pm 1.60	2.232 \pm 0.0686
AGN ($\alpha = 0$)	69.41\pm2.72	0.7961\pm0.0866	62.10\pm3.87	0.7323\pm0.0557	39.56\pm1.39	2.207\pm0.0762

mean as the baseline for $d(\mathbf{s}, \hat{\mathbf{s}})$. Empirically, we find $\alpha = 0.1 - 0.3$ to reduce repetitive tokens without significant sacrifice in sequence modeling performance.

5.2. Training Structure Prediction Model

After training the sequence design model, we proceed to train the structure prediction model. We can employ any existing GNN-based model $p_\phi(\mathbf{s}, \mathbf{x}|\mathcal{G}(s_0, \mathbf{x}_0, \mathbf{c}_{\mathbf{s}, \mathbf{x}}))$ to predict the CDR structure \mathbf{x} by feeding the *generated* sequence \mathbf{s} instead of the *initialized* sequence s_0 as input and using only \mathbf{x} as the output – i.e., $p_\phi(\mathbf{s}, \mathbf{x}|\mathcal{G}(\mathbf{s}, \mathbf{x}_0, \mathbf{c}_{\mathbf{s}, \mathbf{x}}))$.

We highlight that even during training, we use predicted CDR sequence $\hat{\mathbf{s}}$ instead of ground-truth CDR sequence \mathbf{s} as input to the structure prediction model. This is to prevent poor generalization performance during inference, caused by the *covariate shift* (Shimodaira, 2000) between data distribution $p_{\mathcal{D}}(\mathbf{s})$ and model distribution $p_\theta(\mathbf{s}|\mathbf{s}_0, \mathbf{c}_{\mathbf{s}})$.

Implementation. The exact form of the loss function follows that of the chosen GNN-based model, which in our case is MEAN (Kong et al., 2022). However, instead of training the model with structure loss only, we train it with *both* the sequence and structure loss introduced in the original implementation. The inclusion of sequence loss not only ensures that the model fully utilizes $\hat{\mathbf{s}}$ to predict \mathbf{x} but also eases ablation study by keeping both the model architecture and loss function intact. The objective for MEAN is:

$$\mathcal{L}(\phi) = \underbrace{\frac{1}{T} \sum_{t=1}^T \frac{1}{L} \sum_{i=1}^L \ell_{\text{ce}}(\mathbf{p}_i^{(t)}, s_i)}_{\text{Sequence Loss}} + \underbrace{\frac{1}{L} \sum_{i=1}^L \ell_{\text{huber}}(\hat{x}_i, x_i)}_{\text{Structure Loss}} \quad (6)$$

where T is the number of iterations, L is the the total number of residues, $\mathbf{p}_i^{(t)}, s_i$ are predicted/true tokens of i th residue, and \hat{x}_i, x_i are predicted/true backbone coordinates of i th residue.

6. Benchmark Experiments

Task Overview. We evaluate our model on the following benchmarks: **1.** Sequence and Structure Modeling (Section 6.1), **2.** Antigen-binding CDR-H3 Design (Section 6.2),

3. SKEMPI Affinity Optimization (Section 6.3), and **4.** CDR-H3 Design with Docked Templates (Section 6.4).

Baselines. We select LSTM, AR-GNN, and RefineGNN as the autoregressive baselines and MEAN as the non-autoregressive baseline. LSTM is a sequence-only model that consists of an encoder, a decoder, and a cross-attention layer in between. AR-GNN is a fully autoregressive graph generation model from Jin et al. (2020), adapted for antibody design. RefineGNN constructs an E(3)-invariant graph and processes it through message-passing networks (MPN). For all autoregressive baselines, we use the implementations provided in Jin et al. (2021). Unlike these models, MEAN adopts an iterative full-shot decoding scheme, includes more context (e.g., light chain, antigen), and constructs an E(3)-equivariant graph to fully capture the geometry of the antibody-antigen complex. We have not included Verma et al. (2023) and Martinkus et al. (2023) as our baselines since their training codes are publicly unavailable. For a fair comparison, we set the hyperparameters as provided in the original papers (Appendix C).

AGN Setup. We use the ESM2-650M + MEAN combination for all benchmark experiments. We highlight that in this section, we set $\alpha = 0$ in Equation (4) to focus on AGN’s high modeling capacity, yet revisit the experiments with $\alpha > 0$ in Section 7 to demonstrate that our regularization term can address the token repetition problem. We train ESM2-650M for 30 epochs and MEAN for 20 epochs, with the latter following MEAN’s default settings in Kong et al. (2022). For testing, we use the checkpoint with the best validation AAR and lowest validation loss, respectively. The hyperparameter details are provided in Appendix C.

6.1. Sequence and Structure Modeling

In this task, we evaluate the models’ abilities to learn the CDR sequence-structure joint distribution.

Data. Following Kong et al. (2022), we select 3977 IMGT-numbered (Lefranc et al., 2003) complexes from Structural Antibody Database (SABDab) (Dunbar et al., 2014) that contain the full heavy chain, light chain, and antigen sequence and structure. We then split the complexes into train, validation, and test sets according to the CDR clusterings. Specifically, we use MMseqs2 (Steinegger & Söding, 2017) to

Table 2. AAR(\uparrow), CoSim(\uparrow), TM-score(\uparrow), and RMSD(\downarrow) on RAbD benchmark for Antigen-Binding CDR-H3 Design. AGN outperforms baselines on all metrics.

	AAR	CoSim	TM-score	RMSD
LSTM	16.15	0.5462	-	-
AR-GNN	18.85	0.5963	0.9630	3.561
RefineGNN	26.33	0.5797	0.9648	1.803
MEAN	37.15	0.5832	0.9806	1.821
AGN ($\alpha = 0$)	40.45	0.6044	0.9830	1.792

assign antibodies with CDR sequence identity above 40% to the same cluster, where the sequence identity is computed by the BLOSUM62 substitution matrix (Henikoff & Henikoff, 1992). Then we conduct a 10-fold cross-validation by splitting the clusters into a ratio of 8:1:1 for train/valid/test sets, respectively. Detailed statistics of the 10-fold dataset splits are provided in Appendix F.

Metrics. We evaluate the models with amino acid recovery (AAR) and root mean squared deviation (RMSD). The AAR is defined as $AAR(s, \hat{s}) = \sum_{i=1}^L \mathbb{I}(s_i = \hat{s}_i) / L$, where \hat{s} is the generated CDR sequence and s is the ground-truth CDR sequence. The RMSD is defined by comparing C_α coordinates of generated and ground-truth CDR structures.

Results. Table 1 shows that our model significantly outperforms all baselines on both sequence and structure metrics. Compared to MEAN, the previous state-of-the-art model, we show 17.00%, 27.12%, and 8.38% improvement in CDR-H1, CDR-H2, and CDR-H3 AARs, respectively. This shows that leveraging pLM is particularly important in antibody sequence design, as it can exploit the sequential evolutionary knowledge to model CDR sequences. Also, MEAN in AGN exhibits lower RMSD than the stand-alone MEAN, even though they have the same architecture and were trained with the same loss function. We attribute this to the fact that our model follows Anfinsen’s dogma, which we demonstrate in Section 8.

6.2. Antigen-binding CDR-H3 Design

Here, we assess the models’ abilities to design CDR-H3 of the RosettaAntibodyDesign (RAbD) dataset, a benchmark containing 60 diverse antibody-antigen complexes curated by Adolf-Bryfogle et al. (2018).

Data. We use the SAbDab dataset as the train/validation set while using the RAbD dataset as the test set. To properly test the models’ generalization abilities, we first eliminate antibodies in SAbDab whose CDR-H3 sequences are in the same cluster as the RAbD dataset. Then we split the remaining clusters into train and validation sets with a ratio of 9:1. This gives 3418 and 382 antibodies for the training and validation sets, respectively.

Metrics. In addition to AAR and RMSD, we include cosine similarity (abbreviated CoSim) and TM-score (Zhang &

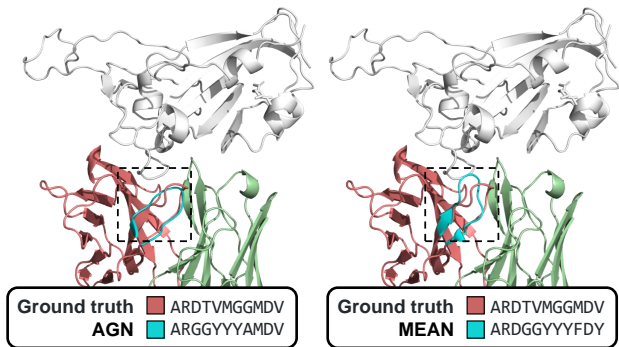


Figure 4. Antigen-binding CDR-H3 of PDB 2dd8 modeled by AGN (left) and MEAN (right). AGN shows higher sequence and structure modeling capacity than MEAN.

Skolnick, 2004; Xu & Zhang, 2010) to evaluate the sequence composition similarity and global structural similarity.

Results. As shown in Table 2, AGN outperforms all baselines in both sequence and structure metrics. In particular, AGN is the only model to exceed AAR of 40%, supporting the use of pre-trained pLMs for antibody sequence design. Also, the MEAN in AGN achieves a higher TM-score and lower RMSD than the stand-alone MEAN, even though the two models assume the same architecture and loss function. Again, we associate the high structural performance to the adoption of Anfinsen’s GM, demonstrated in Section 8.

To better illustrate the CDR-H3 modeling capacity of AGN, in Figure 4, we visualize an antibody (PDB 2dd8) modeled by AGN (left) and MEAN (right). As one can see, AGN closely models the ground-truth CDR-H3 loop structure with an RMSD of 1.202, whereas MEAN shows greater structural deviation with an RMSD of 1.626. Moreover, AGN closely models the ground truth sequence with an AAR of 45.00%, while MEAN exhibits an AAR of 36.36%. In particular, while AGN successfully recovers the end sequence “MDV”, MEAN tends to overfit to “FDY”, the more common ending sequence in the SAbDab training dataset. This again demonstrates that pre-trained pLMs can improve antibody sequence design, preventing overfitting to the small antibody dataset.

6.3. SKEMPI Affinity Optimization

The goal of this task is to optimize the binding affinity of a given antibody-antigen complex by re-designing the CDR-H3 sequence and structure. As an overview, we pre-train the models on the SAbDab dataset and fine-tune them with the ITA algorithm (Yang et al., 2020) on the SKEMPI V2.0 dataset (Jankauskaitė et al., 2019). To evaluate the change in binding affinity $\Delta\Delta G$, we use the official checkpoint of the oracle f from Shan et al. (2022).

Data. The pre-training data is the SAbDab dataset split into training and validation sets with a ratio of 9:1 based on CDR-

Table 3. Change in binding affinity $\Delta\Delta G(\downarrow)$ on SKEMPI dataset. AGN generates re-designs with the highest binding affinities on average.

	Random*	AR-GNN	RefineGNN	MEAN	AGN
$\Delta\Delta G$	+1.520	-2.279	-5.437	-7.199	-8.454

H3 clusters. To ensure an accurate $\Delta\Delta G$ prediction, the fine-tuning dataset is a subset of the SKEMPI V2.0 dataset used to train the oracle f ; this amounts to 53 antibody-antigen complexes, following Kong et al. (2022).

Oracle. We use an attention-based geometric neural network f from Shan et al. (2022) to predict the change in binding affinity. Specifically, given an original antibody-antigen complex \mathcal{AB} and mutated antibody-antigen complex $\hat{\mathcal{A}}\mathcal{B}$, $f(\mathcal{AB}, \hat{\mathcal{A}}\mathcal{B}) = \Delta G(\hat{\mathcal{A}}\mathcal{B}) - \Delta G(\mathcal{AB}) = \Delta\Delta G$ such that $f < 0$ indicates an improvement in binding affinity. We assume that the oracle f is cheap to evaluate, using it both during ITA-based fine-tuning and evaluation.

ITA-based fine-tuning. Following Kong et al. (2022), we adopt the ITA algorithm adjusted for continuous properties. The algorithm consists of two parts – (1) augmenting the dataset and (2) training the model on the augmented dataset. To augment the dataset \mathcal{D} , we select an antibody-antigen complex from \mathcal{D} and generate $\mathcal{M} = 20$ candidate structures with the model. If a candidate is valid and exhibits $f < 0$, we add it to \mathcal{D} and form the augmented dataset \mathcal{Q} . Then, we fine-tune the model on \mathcal{Q} . We repeat this two-step process for $T = 20$ iterations. The details of this algorithm are in Appendix G.

Evaluation. For each antibody-antigen complex in the SKEMPI V2.0 dataset, we generate 100 candidate re-designs and save only the best-scoring complex. We then take an average of the best scores across the dataset.

Results. Table 3 shows that AGN achieves minimum $\Delta\Delta G$, demonstrating its ability to generate antibody re-designs with highest binding affinities. In particular, AGN outperforms MEAN with the same structure prediction network, a performance gap we ascribe to our pipeline (Section 8). For better comparison, we also provide the effect of random mutation from Kong et al. (2022), denoted Random*.

6.4. CDR-H3 Design with Docked Templates

Here, we explore a more challenging setting where both CDR-H3 and the binding complex are unknown. The goal of this task is to generate CDR-H3 designs with higher binding affinities in this challenging setting.

Data. We use the same train/valid/test splits from Section 6.2, yet modify the RAbD test set to create docked templates. More concretely, we first segregate each antibody-antigen complex into a CDR-H3-removed antibody and

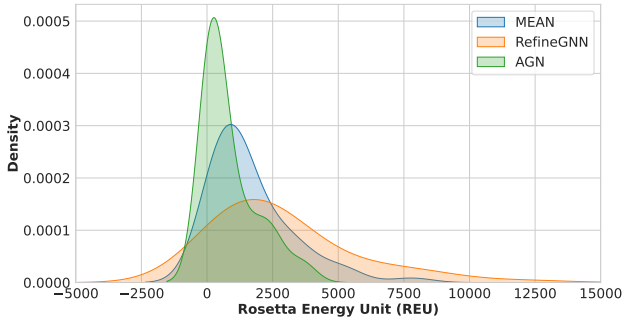


Figure 5. Binding affinity distribution of antibodies re-designed on docked templates. Lower energy (REU) is better. AGN consistently generates structures with high binding affinities.

antigen, which is then used to generate 10,000 docked templates with MEGADOCK (Ohue, 2023). Among them, we include only the top-10 scoring docked templates in the test set.

Evaluation. We prepare the best validation checkpoints from Section 6.2 and generate CDR-H3 re-design for each docked template in the test set. We then evaluate the binding affinities of the re-designed complexes with pyRosetta (Chaudhury et al., 2010) including the side-chain packing. Considering the risk of docking inaccuracy, we report the binding affinities of the top-scoring re-design for each antibody-antigen complex.

Results. We report the distribution of binding affinities in Figure 5. We see that AGN consistently generates structures with higher binding affinities than other models, illustrating its ability to perform well in a more challenging setting.

7. Generating Realistic Sequences for Non-autoregressive Models

To apply non-autoregressive antibody design models in real-world settings, we must resolve the token repetition problem and enforce realistic sequence output. Here, we revisit the experimental setup in Section 6.1 (SAbDab) and Section 6.2 (RAbD) and demonstrate that our regularization term in Equation (4) effectively reduces the percentage of repetitive sequences while maintaining high AAR.

Metrics. As mentioned in Jin et al. (2021), we define a repetitive sequence as a sequence with more than five token repetitions (e.g., ARGYYYYYY). Based on this definition, we develop a new metric called the percentage of repetitive tokens, p_{rep} . Given a model’s sequence predictions $\mathcal{D} = \{\hat{\mathbf{s}}^{(n)}\}_{n=1}^N$, we define $p_{\text{rep}} = \sum_{n=1}^N \mathbb{I}(\hat{\mathbf{s}}^{(n)} \text{ is repetitive}) \times 100\%/N$.

Results. Table 4 demonstrates that AGN trained with the regularization term with $\alpha = 0.12$ reduces p_{rep} without significant sacrifice in performance. To further illustrate the effectiveness of our approach, we dive deeper into CDR-H3 modeling from Section 6.1. As seen in Figure 6, our

Table 4. AAR(\uparrow), RMSD(\downarrow), and p_{rep} (\downarrow) on SAbDab and RAbD benchmarks. Our regularization term (bottom row) reduces token repetition (p_{rep}) while maintaining high performance.

	SAbDab									RAbD		
	CDR-H1			CDR-H2			CDR-H3			CDR-H3		
	AAR	RMSD	p_{rep}	AAR	RMSD	p_{rep}	AAR	RMSD	p_{rep}	AAR	RMSD	p_{rep}
AGN ($\alpha = 0$)	69.41	0.7961	0.2897	62.10	0.7323	0.3362	39.56	2.207	15.55	40.45	1.792	11.67
AGN ($\alpha = 0.12$)	68.84	0.7952	0.2897	61.36	0.7552	0.2799	39.36	2.228	12.69	39.78	1.702	10.00

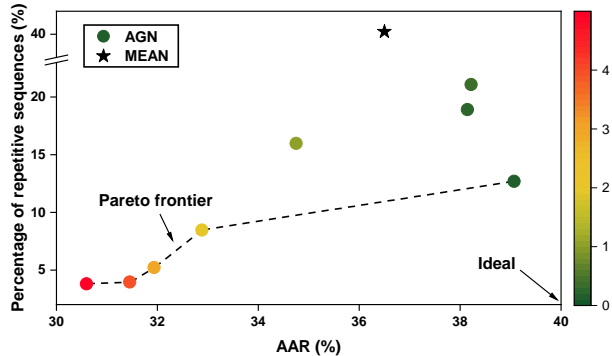


Figure 6. Effect of α on AAR and p_{rep} . Bottom-right is better. AGN establishes a Pareto frontier over MEAN.

method allows a trade-off between high AAR and low p_{rep} by controlling the hyperparameter α . This flexibility allows freedom of choice between a model with high sequence modeling capacity and high realism. Also, AGN establishes a Pareto frontier over MEAN, with both higher AAR and lower p_{rep} . While MEAN shows 40.22% p_{rep} at 36.5% AAR, our approach allows for a much lower p_{rep} with higher AAR (dark green points in Figure 6). We can further reduce p_{rep} by increasing α while maintaining AAR above 30%, as required for CDR design models (Melnik et al., 2022; Weitzner et al., 2015).

8. Ablations

Thus far, we have validated that the ESM2-650M + MEAN combination outperforms other models in benchmark experiments. Here, we demonstrate that other GNN-based models (e.g., RefineGNN, AR-GNN) show performance improvement when embedded into the AGN pipeline.

Data. We revisit the benchmark experiments in Section 6.1 (SAbDab) and Section 6.2 (RAbD) with a focus on CDR-H3 region. For the SAbDab dataset, we randomly select fold 0 from the 10 cross-validation splits (Appendix F).

Baselines. We select AR-GNN, RefineGNN, and MEAN as our baselines. We also create the AGN variants by using each model as the structure prediction network $p_{\phi}(\mathbf{s}, \mathbf{x} | \mathcal{G}(\mathbf{s}, \mathbf{x}_0, \mathbf{c}_{\mathbf{s}, \mathbf{x}}))$. We fix the pLM to ESM2-650M.

Training. We train the baselines with the objectives proposed in their original papers (Jin et al., 2021; Kong et al., 2022). For the AGN variants, we train ESM2-650M with

Table 5. Benchmark results of the GNN-based models and their AGN variants. AGN variants improve both AAR and RMSD.

	SAbDab		RAbD	
	AAR	RMSD	AAR	RMSD
AR-GNN	17.47	3.638	18.81	3.237
AGN(AR-GNN)	41.32	2.807	40.45	3.199
RefineGNN	23.49	2.173	22.43	1.716
AGN(RefineGNN)	41.32	2.000	40.45	1.581
MEAN	35.39	2.188	37.15	1.686
AGN(MEAN)	41.32	2.180	40.45	1.672

the cross-entropy objective and each structure prediction model with the same objective as the baseline. To fully reveal the benefit of our pipeline, we train all models to their full capacity by setting the training epochs to 9999 and patience to 10.

Results. Table 5 highlights the need to (1) leverage pLMs and (2) adopt Anfinsen’s dogma for high performance. First, the AGN variants show higher AARs than their counterparts, exemplifying the importance of using pLMs for antibody sequence design. Second, the AGN variants exhibit lower RMSD than their counterparts, when their only difference in GNNs is whether or not they are embedded within Anfinsen’s GM (Figure 1B). This implies that following Anfinsen’s dogma contributes to high structure modeling performance.

In Appendix H, we further explore the importance of pre-trained pLMs by comparing fine-tuned pLMs to those trained from scratch.

9. Conclusion

In this paper, we introduce AGN, a flexible graphical model for antibody sequence-structure co-design. AGN decouples sequence and structure generation, thereby utilizing pLM and following Anfinsen’s dogma. Our model outperforms all baselines by a large margin in generative tasks, affinity optimization, and CDR-H3 design on docked templates. We also introduce a composition-based regularization term that resolves the token repetition problem of non-autoregressive models. With our approach, one can easily control the trade-off between high AAR and low token repetition with the hyperparameter α . We validate that this approach effectively reduces token repetition while maintaining high AAR.

References

- Adolf-Bryfogle, J., Kalyuzhnyi, O., Kubitz, M., Weitzner, B. D., Hu, X., Adachi, Y., Schief, W. R., and Dunbrack Jr, R. L. Rosettaantibodydesign (rabd): A general framework for computational antibody design. *PLoS computational biology*, 14(4):e1006112, 2018.
- Akbar, R., Robert, P. A., Weber, C. R., Widrich, M., Frank, R., Pavlović, M., Scheffer, L., Chernigovskaya, M., Snapkov, I., Slabodkin, A., et al. In silico proof of principle of machine learning-based antibody design at unconstrained scale. In *MAbs*, volume 14, pp. 2031482. Taylor & Francis, 2022.
- Anfinsen, C. B. Principles that govern the folding of protein chains. *Science*, 181(4096):223–230, 1973.
- Ba, J. L., Kiros, J. R., and Hinton, G. E. Layer normalization. *arXiv preprint arXiv:1607.06450*, 2016.
- Chaudhury, S., Lyskov, S., and Gray, J. J. Pyrosetta: a script-based interface for implementing molecular modeling algorithms using rosetta. *Bioinformatics*, 26(5):689–691, 2010.
- Dauparas, J., Anishchenko, I., Bennett, N., Bai, H., Ragotte, R. J., Milles, L. F., Wicky, B. I., Courbet, A., de Haas, R. J., Bethel, N., et al. Robust deep learning-based protein sequence design using proteinmpnn. *Science*, 378(6615):49–56, 2022.
- Devlin, J., Chang, M.-W., Lee, K., and Toutanova, K. Bert: Pre-training of deep bidirectional transformers for language understanding. *arXiv preprint arXiv:1810.04805*, 2018.
- Dunbar, J., Krawczyk, K., Leem, J., Baker, T., Fuchs, A., Georges, G., Shi, J., and Deane, C. M. Sabdab: the structural antibody database. *Nucleic acids research*, 42(D1):D1140–D1146, 2014.
- Elnaggar, A., Heinzinger, M., Dallago, C., Rehawi, G., Wang, Y., Jones, L., Gibbs, T., Feher, T., Angerer, C., Steinegger, M., et al. Prottrans: Toward understanding the language of life through self-supervised learning. *IEEE transactions on pattern analysis and machine intelligence*, 44(10):7112–7127, 2021.
- Ferruz, N., Schmidt, S., and Höcker, B. Protgpt2 is a deep unsupervised language model for protein design. *Nature communications*, 13(1):4348, 2022.
- Fu, C., Fu, C., and Michael, M. *Handbook of simulation optimization*. Springer, 2015.
- Gao, Z., Tan, C., Chacón, P., and Li, S. Z. Pifold: Toward effective and efficient protein inverse folding. *arXiv preprint arXiv:2209.12643*, 2022.
- Ghazvininejad, M., Levy, O., Liu, Y., and Zettlemoyer, L. Mask-predict: Parallel decoding of conditional masked language models. *arXiv preprint arXiv:1904.09324*, 2019.
- Gu, J., Bradbury, J., Xiong, C., Li, V. O., and Socher, R. Non-autoregressive neural machine translation. *arXiv preprint arXiv:1711.02281*, 2017.
- He, L., Zhang, S., Wu, L., Xia, H., Ju, F., Zhang, H., Liu, S., Xia, Y., Zhu, J., Deng, P., et al. Pre-training co-evolutionary protein representation via a pairwise masked language model. *arXiv preprint arXiv:2110.15527*, 2021.
- Hendrycks, D. and Gimpel, K. Gaussian error linear units (gelus). *arXiv preprint arXiv:1606.08415*, 2016.
- Henikoff, S. and Henikoff, J. G. Amino acid substitution matrices from protein blocks. *Proceedings of the National Academy of Sciences*, 89(22):10915–10919, 1992.
- Hu, E. J., Shen, Y., Wallis, P., Allen-Zhu, Z., Li, Y., Wang, S., Wang, L., and Chen, W. Lora: Low-rank adaptation of large language models. *arXiv preprint arXiv:2106.09685*, 2021.
- Ingraham, J., Garg, V., Barzilay, R., and Jaakkola, T. Generative models for graph-based protein design. *Advances in neural information processing systems*, 32, 2019.
- Jankauskaitė, J., Jiménez-García, B., Dapkūnas, J., Fernández-Recio, J., and Moal, I. H. Skempi 2.0: an updated benchmark of changes in protein-protein binding energy, kinetics and thermodynamics upon mutation. *Bioinformatics*, 35(3):462–469, 2019.
- Jin, S., Sun, Y., Liang, X., Gu, X., Ning, J., Xu, Y., Chen, S., and Pan, L. Emerging new therapeutic antibody derivatives for cancer treatment. *Signal Transduction and Targeted Therapy*, 7(1):39, 2022a.
- Jin, W., Barzilay, R., and Jaakkola, T. Multi-objective molecule generation using interpretable substructures. In *International conference on machine learning*, pp. 4849–4859. PMLR, 2020.
- Jin, W., Wohlwend, J., Barzilay, R., and Jaakkola, T. Iterative refinement graph neural network for antibody sequence-structure co-design. *arXiv preprint arXiv:2110.04624*, 2021.
- Jin, W., Barzilay, R., and Jaakkola, T. Antibody-antigen docking and design via hierarchical equivariant refinement. *arXiv preprint arXiv:2207.06616*, 2022b.
- Jing, B., Eismann, S., Suriana, P., Townshend, R. J., and Dror, R. Learning from protein structure with geometric vector perceptrons. *arXiv preprint arXiv:2009.01411*, 2020.

- Kaplan, J., McCandlish, S., Henighan, T., Brown, T. B., Chess, B., Child, R., Gray, S., Radford, A., Wu, J., and Amodei, D. Scaling laws for neural language models. *arXiv preprint arXiv:2001.08361*, 2020.
- Kong, X., Huang, W., and Liu, Y. Conditional antibody design as 3d equivariant graph translation. *arXiv preprint arXiv:2208.06073*, 2022.
- Langley, P. Crafting papers on machine learning. In Langley, P. (ed.), *Proceedings of the 17th International Conference on Machine Learning (ICML 2000)*, pp. 1207–1216, Stanford, CA, 2000. Morgan Kaufmann.
- Lapidoth, G. D., Baran, D., Pszolla, G. M., Norn, C., Alon, A., Tyka, M. D., and Fleishman, S. J. Abdesign: A n algorithm for combinatorial backbone design guided by natural conformations and sequences. *Proteins: Structure, Function, and Bioinformatics*, 83(8):1385–1406, 2015.
- Lefranc, M.-P., Pommié, C., Ruiz, M., Giudicelli, V., Foulquier, E., Truong, L., Thouvenin-Contet, V., and Lefranc, G. Imgt unique numbering for immunoglobulin and t cell receptor variable domains and ig superfamily v-like domains. *Developmental & Comparative Immunology*, 27(1):55–77, 2003.
- Li, T., Pantazes, R. J., and Maranas, C. D. Optmaven—a new framework for the de novo design of antibody variable region models targeting specific antigen epitopes. *PLoS one*, 9(8):e105954, 2014.
- Lin, Z., Akin, H., Rao, R., Hie, B., Zhu, Z., Lu, W., Smetanin, N., Verkuil, R., Kabeli, O., Shmueli, Y., et al. Evolutionary-scale prediction of atomic-level protein structure with a language model. *Science*, 379(6637): 1123–1130, 2023.
- Liu, G., Zeng, H., Mueller, J., Carter, B., Wang, Z., Schilz, J., Horny, G., Birnbaum, M. E., Ewert, S., and Gifford, D. K. Antibody complementarity determining region design using high-capacity machine learning. *Bioinformatics*, 36(7):2126–2133, 2020.
- Luo, S., Su, Y., Peng, X., Wang, S., Peng, J., and Ma, J. Antigen-specific antibody design and optimization with diffusion-based generative models for protein structures. *Advances in Neural Information Processing Systems*, 35: 9754–9767, 2022.
- Martinkus, K., Ludwiczak, J., Cho, K., Lian, W.-C., Lafrance-Vanasse, J., Hotzel, I., Rajpal, A., Wu, Y., Bonneau, R., Gligorijevic, V., et al. Abdiffuser: Full-atom generation of in-vitro functioning antibodies. *arXiv preprint arXiv:2308.05027*, 2023.
- McDermott, M., Yap, B., Hsu, H., Jin, D., and Szolovits, P. Adversarial contrastive pre-training for protein sequences. *arXiv preprint arXiv:2102.00466*, 2021.
- Meier, J., Rao, R., Verkuil, R., Liu, J., Sercu, T., and Rives, A. Language models enable zero-shot prediction of the effects of mutations on protein function. *Advances in Neural Information Processing Systems*, 34:29287–29303, 2021.
- Melnyk, I., Chenthamarakshan, V., Chen, P.-Y., Das, P., Dhurandhar, A., Padhi, I., and Das, D. Reprogramming large pretrained language models for antibody sequence infilling. *arXiv preprint arXiv:2210.07144*, 2022.
- Nambiar, A., Heflin, M., Liu, S., Maslov, S., Hopkins, M., and Ritz, A. Transforming the language of life: transformer neural networks for protein prediction tasks. In *Proceedings of the 11th ACM international conference on bioinformatics, computational biology and health informatics*, pp. 1–8, 2020.
- Ohue, M. Megadock-on-colab: an easy-to-use protein-protein docking tool on google colaboratory. *BMC Research Notes*, 16(1):229, 2023.
- Pantazes, R. and Maranas, C. D. Optcdr: a general computational method for the design of antibody complementarity determining regions for targeted epitope binding. *Protein Engineering, Design & Selection*, 23(11):849–858, 2010.
- Rao, R., Bhattacharya, N., Thomas, N., Duan, Y., Chen, P., Canny, J., Abbeel, P., and Song, Y. Evaluating protein transfer learning with tape. *Advances in neural information processing systems*, 32, 2019.
- Raybould, M. I., Marks, C., Krawczyk, K., Taddese, B., Nowak, J., Lewis, A. P., Bujotzek, A., Shi, J., and Deane, C. M. Five computational developability guidelines for therapeutic antibody profiling. *Proceedings of the National Academy of Sciences*, 116(10):4025–4030, 2019.
- Rives, A., Goyal, S., Meier, J., Guo, D., Ott, M., Zitnick, C. L., Ma, J., and Fergus, R. Biological structure and function emerge from scaling unsupervised learning to 250 million protein sequences. *bioRxiv*, 2019.
- Rives, A., Meier, J., Sercu, T., Goyal, S., Lin, Z., Liu, J., Guo, D., Ott, M., Zitnick, C. L., Ma, J., et al. Biological structure and function emerge from scaling unsupervised learning to 250 million protein sequences. *Proceedings of the National Academy of Sciences*, 118(15):e2016239118, 2021.
- Saka, K., Kakuzaki, T., Metsugi, S., Kashiwagi, D., Yoshida, K., Wada, M., Tsunoda, H., and Teramoto, R. Antibody design using lstm based deep generative model from phage display library for affinity maturation. *Scientific reports*, 11(1):5852, 2021.

- Shan, S., Luo, S., Yang, Z., Hong, J., Su, Y., Ding, F., Fu, L., Li, C., Chen, P., Ma, J., et al. Deep learning guided optimization of human antibody against sars-cov-2 variants with broad neutralization. *Proceedings of the National Academy of Sciences*, 119(11):e2122954119, 2022.
- Shimodaira, H. Improving predictive inference under covariate shift by weighting the log-likelihood function. *Journal of statistical planning and inference*, 90(2):227–244, 2000.
- Steinegger, M. and Söding, J. Mmseqs2 enables sensitive protein sequence searching for the analysis of massive data sets. *Nature biotechnology*, 35(11):1026–1028, 2017.
- Suzek, B. E., Wang, Y., Huang, H., McGarvey, P. B., Wu, C. H., and Consortium, U. Uniref clusters: a comprehensive and scalable alternative for improving sequence similarity searches. *Bioinformatics*, 31(6):926–932, 2015.
- Tan, C., Gao, Z., Xia, J., Hu, B., and Li, S. Z. Generative de novo protein design with global context. *arXiv preprint arXiv:2204.10673*, 2022.
- Verkuil, R., Kabeli, O., Du, Y., Wicky, B. I., Milles, L. F., Dauparas, J., Baker, D., Ovchinnikov, S., Sercu, T., and Rives, A. Language models generalize beyond natural proteins. *bioRxiv*, pp. 2022–12, 2022.
- Verma, Y., Heinonen, M., and Garg, V. Abode: Ab initio antibody design using conjoined odes. *arXiv preprint arXiv:2306.01005*, 2023.
- Weitzner, B. D., Dunbrack, R. L., and Gray, J. J. The origin of cdr h3 structural diversity. *Structure*, 23(2):302–311, 2015.
- Xiao, Y., Qiu, J., Li, Z., Hsieh, C.-Y., and Tang, J. Modeling protein using large-scale pretrain language model. *arXiv preprint arXiv:2108.07435*, 2021.
- Xu, J. and Zhang, Y. How significant is a protein structure similarity with tm-score= 0.5? *Bioinformatics*, 26(7): 889–895, 2010.
- Yang, K., Jin, W., Swanson, K., Barzilay, R., and Jaakkola, T. Improving molecular design by stochastic iterative target augmentation. In *International Conference on Machine Learning*, pp. 10716–10726. PMLR, 2020.
- Zhang, Y. and Skolnick, J. Scoring function for automated assessment of protein structure template quality. *Proteins: Structure, Function, and Bioinformatics*, 57(4):702–710, 2004.
- Zheng, Z., Deng, Y., Xue, D., Zhou, Y., Ye, F., and Gu, Q. Structure-informed language models are protein designers. *bioRxiv*, pp. 2023–02, 2023.

A. Related Work

Protein Design. Due to their relevance, methods in protein design can offer valuable insights into antibody design. [Ingraham et al. \(2019\)](#) represents the protein structure with a k-nearest neighbor graph and applies a Transformer-based encoder-decoder model to predict the sequences autoregressively. To fully capture the complex geometry within the graphs, [Jing et al. \(2020\)](#) introduces geometric vector perceptrons that can replace MLPs in GNNs. [Tan et al. \(2022\)](#) introduces an additional global module that captures the global context of the protein structure. To enable an application to a wide range of protein design problems, [Dauparas et al. \(2022\)](#) adopts an order-agnostic autoregressive model with random decoding orders. Instead, [Gao et al. \(2022\)](#) adopts a one-shot decoding scheme and drastically improves the inference speed. Recently, [Zheng et al. \(2023\)](#) showed state-of-the-art performance by repurposing a protein language model with a lightweight structural adapter.

Protein Language Models. Parallel to large language models (LLMs), the abundance of protein sequence data spurred the emergence of protein language models (pLMs). Most works on pLMs adopt the masked language modeling (MLM) objective to pre-train a Transformer-based language model ([Rives et al., 2021](#); [Lin et al., 2023](#); [Rao et al., 2019](#); [Elnaggar et al., 2021](#); [Nambiar et al., 2020](#); [Xiao et al., 2021](#)). Some works propose alternative training objectives, such as pairwise masked language modeling ([He et al., 2021](#)), adversarial contrastive training ([McDermott et al., 2021](#)), and causal language modeling ([Ferruz et al., 2022](#)). The pre-trained pLMs are useful in a variety of downstream tasks, including but not limited to protein structure prediction ([Lin et al., 2023](#)), mutation effect prediction ([Meier et al., 2021](#)), and *de novo* protein design ([Verkuil et al., 2022](#)). In this work, we show that pLMs are also useful in antibody sequence-structure co-design.

B. Steps to Derive Anfinsen’s Graphical Model

Here, we detail a step-by-step guide to derive Anfinsen’s GM in Figure 1B. We start from the GM of GNN-based methods in Figure 1A.

1. (Figure 7A) Split the node h into nodes h_1 and h_2 .
2. (Figure 7B) Remove any edges that encode $x \rightarrow s$, which is the reverse of the intended data-generating process $s \rightarrow x$. To achieve this, we first remove edge $x_0 \rightarrow h_1$ so that x_0 does not influence s . We also remove edge $h_1 \rightarrow x$ since h_1 now contains sequential information only. Since h_2 takes x_0 as input, we should also remove the edge $h_2 \rightarrow s$ and prevent the flow from x_0 to s .
3. (Figure 7C) Adjust edges to reflect the causal relationship $s \rightarrow x$. To do this, we need to add edge $s \rightarrow h_2$ so that sequence s can be used to generate structure x . We can also remove edge $s_0 \rightarrow h_2$ since s contains necessary sequential information for structure prediction.

Rearranging and renaming the nodes for clarity, we get Figure 1B, a GM that encodes Anfinsen’s dogma. This GM first designs the sequence and then predicts the structure, which is the intended data-generation process $s \rightarrow x$.

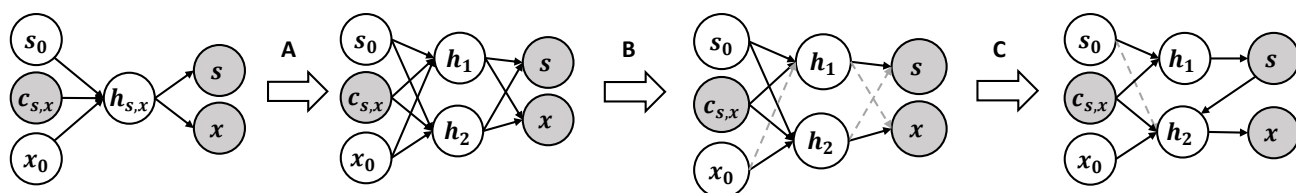


Figure 7. Steps to derive GM that encodes Anfinsen’s dogma. The final GM follows a two-step procedure $s \rightarrow x$.

C. Hyperparameters

Training details for AGN. Table 6 and Table 7 shows the hyperparameters of baselines and pLMs, respectively. All combinations of models (e.g., esm2_t33_650M_UR50D as sequence design model and MEAN as structure prediction model) adopt the hyperparameters stated therein. We fix the pLM to esm2_t33_650M_UR50D in all benchmark experiments, yet resort to smaller models in tasks that require more memories. We train esm2_t33_650M_UR50D for 30 epochs with a batch size limited by a maximum token length of 6000 and train MEAN for 20 epochs with a batch size of 16.

Training details for baselines. To ensure a fair comparison, for RefineGNN and MEAN, we use the hyperparameters and training settings provided in the original papers (Jin et al., 2021; Kong et al., 2022). For LSTM and AR-GNN, we adopted the hyperparameter settings that showed good performance across all experiments.

Code. Our implementation is built upon <https://github.com/facebookresearch/esm>, <https://github.com/BytedProtein/ByProt/tree/main>, <https://github.com/wengong-jin/RefineGNN>, and <https://github.com/THUNLP-MT/MEAN/tree/main>. We deeply appreciate the authors (Lin et al., 2023; Zheng et al., 2023; Jin et al., 2021; Kong et al., 2022) for their contributions to our project.

Machine specs. All models were trained on a machine with 48 CPU cores and 8 NVIDIA Geforce RTX 3090. We have used 1-4 GPUs for all experiments, yet 1 GPU should be sufficient.

Table 6. Hyperparameters for GNN-based baselines.

	LSTM	AR-GNN	RefineGNN	MEAN
Vocab size			25	
Dropout			0.1	
Hidden dim		256		128
Number of layers	4	4	4	3
K neighbors	-	9	9	-
Block size	-	-	4	-
Number of RBF kernels	-	16	16	-
Embed dim	-	-	-	64
Alpha	-	-	-	0.8
Number of iterations	-	-	-	3
Optimizer			Adam	
Learning rate			0.001	

Table 7. Hyperparameters for ESM2 used as the sequence design model.

	esm2_t6_8M_UR50D	esm2_t12_35M_UR50D	esm2_t30_150_UR50D	esm2_t33_650M_UR50D
Vocab size			33	
Embed dim	320	480	640	1280
Number of layers	6	12	30	33
Optimizer			AdamW	
Learning rate			0.001	

D. Effect of Including Antigen Sequence in Context

For all experiments, we fixed the context sequence c_s to the heavy chain framework region. Here, we revisit Section 6.1 and Section 6.2 by including the antigen sequence in c_s . Due to memory limitations, we use a fully fine-tuned ESM2-8M for both experiments.

Table 8. Effect of including the antigen sequence in c_s . AGN performs better when setting c_s to heavy chain framework region only.

	SAbDab			RABD	
	CDR-H1	CDR-H2	CDR-H3	CDR-H3	
	AAR (%)	AAR (%)	AAR (%)	AAR (%)	CoSim
Without antigen	73.45	67.44	41.21	43.86	0.6448
With antigen	72.32	66.85	39.09	41.70	0.6326

Results. Table 8 shows that including antigen in c_s weakens the CDR sequence modeling performance. Since most residues in the antigen do not directly interact with the CDR regions, including all antigen residues in c_s could have challenged CDR sequence modeling.

E. Effect of Sample Recycling on Sequence Quality

One approach to reducing token repetition of non-autoregressive models is recycling tokens for T iterations (Ghazvininejad et al., 2019; Zheng et al., 2023). We here demonstrate that this approach is not effective against antibody design,

Results. As shown in Figure 8A, sample recycling (Ghazvininejad et al., 2019; Zheng et al., 2023) does not reduce token repetition of non-autoregressive models on antibody modeling tasks. It even increases p_{rep} for CDR-H3 from about 15% to 20%. Also, Figure 8B shows that sample recycling even decreases AARs for all CDR regions. Contrary to this approach, our composition-based regularization term effectively reduces p_{rep} while maintaining high AAR, as demonstrated in Section 7.

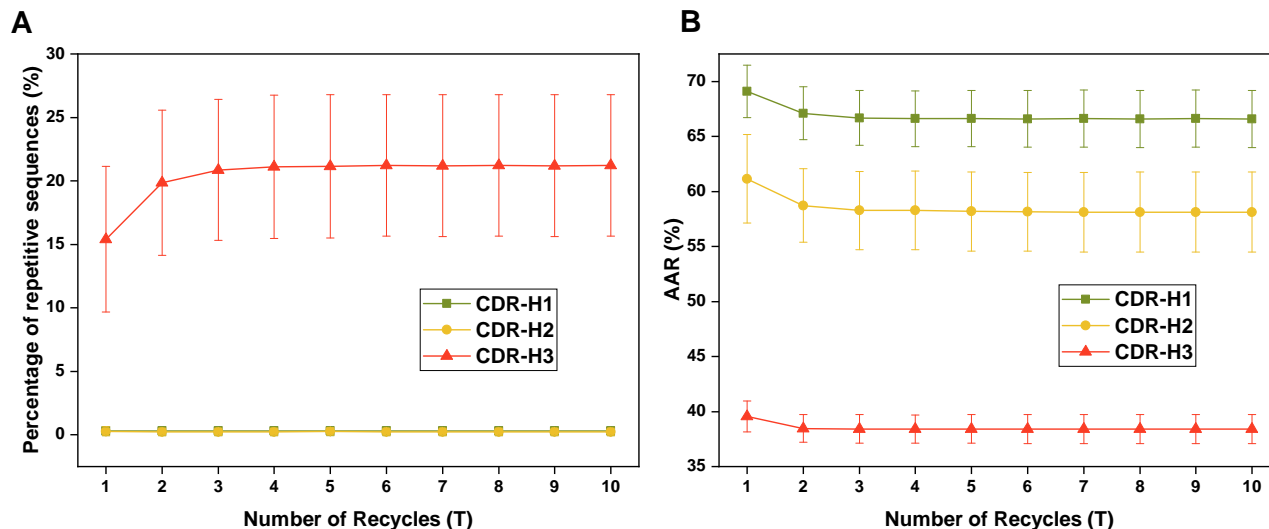


Figure 8. Effect of sample recycling on p_{rep} (left) and AAR (right). (A) Sample recycling does not reduce token repetition for antibody design tasks. (B) Sample recycling even reduces AAR across all CDRs.

F. Data Statistics for Section 6.1

In Table 9, we detail the number of antibodies in each fold for 10-fold cross-validation in Section 6.1. Following Kong et al. (2022), $\forall i = 0, \dots, 9$, we let fold i be the test set, fold $i - 1$ be the validation set, and the remaining folds to be the train set.

Table 9. Number of antibodies in each fold for Sequence and Structure Modeling (Section 6.1)

	CDR-H1	CDR-H2	CDR-H3
fold 0	539	425	390
fold 1	529	366	444
fold 2	269	363	369
fold 3	391	380	389
fold 4	305	392	420
fold 5	523	381	413
fold 6	294	409	403
fold 7	310	369	327
fold 8	472	489	355
fold 9	345	403	467
Total	3977	3977	3977

G. ITA Algorithm for SKEMPI Affinity Optimization

Criterion for validity. We force all generated sequences to satisfy the following constraints: (1) net charge must be in the range $[-2.0, 2.0]$, (2) sequence must not contain N-X-S/T motif, (3) a token should not repeat more than five times (e.g., YYYYYY), (4) perplexity of the sequence must be below 10. The first two constraints ensure that the sequences are developable (Raybould et al., 2019) and the last two constraints ensure that they are realistic (Jin et al., 2021).

Algorithm 1 details the ITA algorithm in Section 6.3, where we have followed Kong et al. (2022) for the implementation.

Algorithm 1 ITA algorithm for SKEMPI affinity optimization

Input: SKEMPI antibody-antigen complex dataset \mathcal{D}

Input: Pre-trained $p_\theta(\mathbf{s}, \mathbf{x}|\mathbf{s}_0, \mathbf{x}_0, \mathbf{c}_{\mathbf{s}, \mathbf{x}})$

Input: top- k candidates to maintain

```

1: Initialize  $\mathcal{Q} \leftarrow \mathcal{D}$ 
2: for  $t = 1, \dots, T$  do
3:   for  $\mathcal{AB} \in \mathcal{D}$  do
4:     Initialize  $\mathcal{C} \leftarrow \emptyset$ , candidate set for  $\mathcal{AB}$ 
5:     for  $i = 1, \dots, M$  do
6:        $(\hat{\mathbf{s}}_i, \hat{\mathbf{x}}_i) \sim p_\theta(\mathbf{s}, \mathbf{x}|\mathbf{s}_0, \mathbf{x}_0, \mathbf{c}_{\mathbf{s}, \mathbf{x}})$ 
7:       Denote  $\hat{\mathcal{A}}_i \leftarrow (\hat{\mathbf{s}}_i, \hat{\mathbf{x}}_i, \mathbf{c}_{\mathbf{s}, \mathbf{x}})$ 
8:       if  $\text{valid}(\hat{\mathcal{A}}_i)$  and  $f(\mathcal{AB}, \hat{\mathcal{A}}_i\mathcal{B}) < 0$  then
9:          $\mathcal{C} \leftarrow \mathcal{C} \cup \{(\hat{\mathcal{A}}_i\mathcal{B}, f(\mathcal{AB}, \hat{\mathcal{A}}_i\mathcal{B}))\}$ 
10:      end if
11:    end for
12:     $\mathcal{Q}[\mathcal{AB}] \leftarrow \mathcal{Q}[\mathcal{AB}] \cup \mathcal{C}$ 
13:    Select top- $k$  elements in  $\mathcal{Q}[\mathcal{AB}]$  by  $f(\cdot, \cdot)$ 
14:  end for
15:  for  $n = 1, \dots, N$  do
16:    Select batch  $\mathcal{B}$  from  $\mathcal{Q}$ 
17:    Update  $\theta \leftarrow \theta - \eta \nabla_\theta \mathcal{L}(\mathcal{B}, \theta)$ 
18:  end for
19: end for

```

H. Ablations on Protein Language Models

Here, we demonstrate that leveraging pre-trained pLMs boosts the performance of AGN by comparing fine-tuned pLMs and those trained from scratch.

Data. We train and test the models following the benchmark experiments Section 6.1 and Section 6.2, denoted SAbDab and RAbD, respectively. We use fold 0 (Table 9) for the SAbDab dataset.

Baselines. We train ESM2-8M, ESM2-35M, and ESM2-150M either from scratch (denoted “scratch” in Table 10) or from pre-trained model weights (denoted “fine-tune” in Table 10). We have omitted ESM2-650M from this experiment due to memory limitations.

Results. Table 10 demonstrate that models fine-tuned from pre-trained checkpoints outperform those trained from scratch across all sequence metrics and datasets. This supports that pre-trained pLMs enhance antibody sequence modeling performance by leveraging sequential evolutionary knowledge learned from general sequence datasets.

Interestingly, Table 10 also shows that antibody sequence modeling performance does not scale with model size. This is consistent with the results in Kaplan et al. (2020), where the usual scaling laws of large language models barely hold for small datasets.

Table 10. Benchmark results of the ESM2 series either trained from scratch or fine-tuned from pre-trained checkpoints. The fine-tuned variants outperform their counterparts in all settings, demonstrating the benefit of pre-trained pLMs for antibody design.

	SAbDab			RAbD	
	CDR-H1	CDR-H2	CDR-H3	CDR-H3	
	AAR (%)	AAR (%)	AAR (%)	AAR (%)	CoSim
ESM2-8M scratch	71.84	67.03	41.12	41.28	0.5679
ESM2-8M fine-tune	73.45	67.44	43.18	43.86	0.6448
ESM2-35M scratch	71.27	67.13	40.03	39.92	0.5949
ESM2-35M fine-tune	71.81	67.32	42.66	42.21	0.6029
ESM2-150M scratch	71.95	68.17	40.40	39.53	0.5893
ESM2-150M fine-tune	72.40	69.08	41.86	42.36	0.6378